DNA Folding: Structural and Mechanical Properties of the Two-Angle Model for Chromatin

Helmut Schiessel,*† William M. Gelbart,† and Robijn Bruinsma*
*Departments of Physics and †Chemistry and Biochemistry, University of California, Los Angeles, Los Angeles, California 90095 USA

ABSTRACT We present a theoretical analysis of the structural and mechanical properties of the 30-nm chromatin fiber. Our study is based on the two-angle model introduced by Woodcock et al. (Woodcock, C. L., S. A. Grigoryev, R. A. Horowitz, and N. Whitaker. 1993. *Proc. Natl. Acad. Sci. USA.* 90:9021–9025) that describes the chromatin fiber geometry in terms of the entry-exit angle of the nucleosomal DNA and the rotational setting of the neighboring nucleosomes with respect to each other. We analytically explore the different structures that arise from this building principle, and demonstrate that the geometry with the highest density is close to the one found in native chromatin fibers under physiological conditions. On the basis of this model we calculate mechanical properties of the fiber under stretching. We obtain expressions for the stress-strain characteristics that show good agreement with the results of recent stretching experiments (Cui, Y., and C. Bustamante. 2000. *Proc. Natl. Acad. Sci. USA.* 97:127–132) and computer simulations (Katritch, V., C. Bustamante, and W. K. Olson. 2000. *J. Mol. Biol.* 295:29–40), and which provide simple physical insights into correlations between the structural and elastic properties of chromatin.

INTRODUCTION

Recently there has been considerable progress both in the visualization (Bednar et al., 1998) and micromanipulation (Cui and Bustamante, 2000) of chromatin fibers. These results constitute an important step toward the understanding of DNA "folding," i.e., the problem of how plant and animal genomes organize themselves into volumes whose linear dimensions are many orders of magnitude smaller than their contour lengths. For instance, human DNA is billions of basepairs (bp) long (about a meter); this length of highly charged (about one fundamental charge per two Angstroms) and hard-to-bend (persistence length of 50 nm) linear polymer must be condensed into chromosomes that fit into cell nuclei whose characteristic size is a micron.

An important part of the condensation process is the complexation of DNA with oppositely charged globular protein (histone) aggregates that have the shape of squat cylinders. These aggregates are octameric complexes consisting of pairs of the four core histones H2A, H2B, H3, and H4. A DNA stretch of 147 bp is wrapped in a 1¾ left-handed superhelical turn around the histone octamer and is connected via a stretch of "linker" DNA to the next such protein spool. Each protein aggregate together with its wrapped DNA composes a nucleosome core particle (cf. Fig. 1) with a radius of ~5 nm and a height of ~6 nm; with its linker DNA it is the fundamental chromatin repeating unit. It carries a large negative electrostatic charge (Khrapunov et al., 1997; Raspaud et al., 1999). Whereas the structure of the core particle has been resolved up to high atomic resolution (Luger et al., 1997), there is still considerable controversy about the nature of the higher-order structures to which they give rise. When stretched, the string of DNA/histone complexes has the appearance of "beads-on-a-string." This basic structure can be seen clearly when chromatin is exposed to very low salt concentrations, and is known as the "10-nm fiber" (Thoma et al., 1979), because the diameter of the core particle is 10 nm. With increasing salt concentration, i.e., heading toward physiological conditions (100 mM), this fiber appears to thicken, attaining a diameter of 30 nm (Widom, 1986). The absence of the extra "linker histones" (H1 or H5) leads to more open structures (Thoma et al., 1979) so it is surmised that the linker histones act near the entry-exit point of the DNA (cf. Fig. 1); they carry an overall positive charge and seem to bind the two strands together, leading to a stem formation (Bednar et al., 1998). Increasing the salt concentration is expected to decrease the entry-exit angle of the stem as it reduces the electrostatic repulsion between the two strands.

Longstanding controversy (van Holde, 1989; Widom, 1989; van Holde and Zlatanova, 1995, 1996) surrounds the structure of this "30-nm fiber," for which there are mainly two competing classes of models: the solenoid models (Finch and Klug, 1976; Thoma et al., 1979; Widom and Klug, 1985), and the zig-zag or crossed-linker models (Woodcock et al., 1993; Horowitz et al., 1994; Leuba et al., 1994; Bednar et al., 1998). In the solenoid model (Fig. 2 *A*) it is assumed that the chain of nucleosomes forms a helical structure with the axis of the core particles being perpendicular to the solenoid axis (the axis of an octamer corresponds to the axis of the superhelical path of the DNA that wraps around it). The DNA entry-exit side faces inward toward the axis of the solenoid. The linker DNA (shown as

Received for publication 31 July 2000 and in final form 17 January 2001.

Address reprint requests to Dr. Helmut Schiessel, Theory Group, Max Planck Institute for Polymer Research, P.O. Box 3148, D-55021 Mainz, Germany. Tel.: 49-6131-379-165; Fax: 49-6131-379-340; E-mail: heli@mpip-mainz.mpg.de.

H. Schiessel's present address is Max Planck Institute.

R. Bruinsma's present address is Instituut-Lorentz for Theoretical Physics, Universiteit Leiden, Postbus 9506, 2300 RA Leiden, The Netherlands.

0006-3495/01/04/1940/17 $2.00

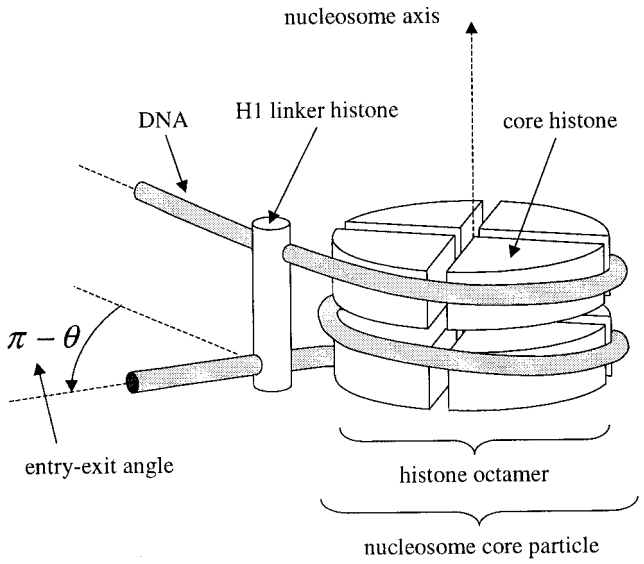

FIGURE 1 Schematic representation of the nucleosome. Eight core histones aggregate into the histone octamer that acts as a cylindrical spool around which the DNA is wound in 1 ¾ turns. The linker histone is also depicted that acts at the entry-exit point of the DNA. The entry-exit angle $\pi - \theta$ of the linker DNA is one of the angles defining the two-angle model.

a dashed curve at the top of Fig. 2 *A*) is required to be bent in order to connect neighboring nucleosomes in the solenoid. The other class of models posits straight linkers that connect nucleosomes located on opposite sides of the fiber. This results in a three-dimensional zig-zag-like pattern of the linker (Fig. 2 *B*).

Images obtained by electron cryomicroscopy should in principle be able to distinguish between the structural features proposed by the different models mentioned above (Bednar et al., 1998). The micrographs show a zig-zag motif at lower salt concentrations and they indicate that the chromatin fiber becomes more and more compact when the ionic strength is raised toward the physiological value. However,

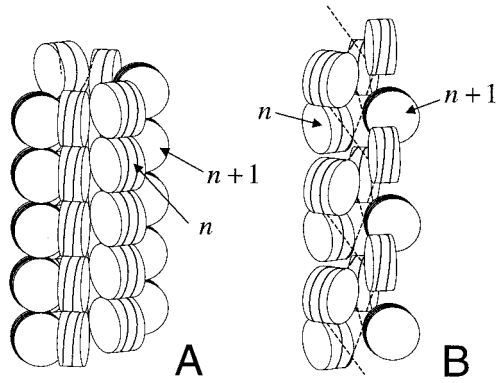

FIGURE 2 The two competing models for the 30-fiber. (*A*) The solenoid model and (*B*) the crossed linker model (see text).

for these denser fibers it is still not possible to detect the exact linker geometry (see Note 1 at end of text).

An important experimental achievement was the stretching of a single chromatin fiber via micromanipulation (Cui and Bustamante, 2000). The "force-extension" measurements show a rich behavior of the mechanical properties as a function of the ionic strength. At low ionic strength (5 mM NaCl) the force-extension curves are reversible as long as the tension does not exceed 20 pN. For higher tension levels ($\gtrsim$20 pN) there are irreversible changes that lead to an increase of the fiber length, probably due to the loss of linker histones and/or histone octamers. At high ionic strength (40 and 150 mM NaCl) a 5-pN plateau in the force extension curve was found (see Note 2). The authors interpreted their results as indicating a coexistence between "swollen" and "condensed" parts of the fiber. In order to reproduce the force-extension curves, Katritch et al. performed Monte Carlo simulations (Katritch et al., 2000) based on a geometrical "two-angle" model introduced by Woodcock et al. for the 30-nm fiber (Woodcock et al., 1993) combined with the worm-like chain (WLC) Hamiltonian for the linkers. The WLC is widely used for predicting the mechanical properties of naked DNA. The low-salt behavior could be reproduced for several sets of angles and bond lengths of the model, demonstrating both that it is a reasonable model and that it is not possible to deduce a unique structure from the measured response of the fiber under stretching. Katritch et al. found that an internucleosomal attraction of $\sim$3 kT might explain the experimentally observed plateau in the force-extension profile. The biological importance of these results lies in the fact that significant changes can be achieved in the degree of chromatin condensation with only modest levels of external stress. The fact that chromatin at physiological salt concentrations apparently can exist in two alternative forms that interconvert under low levels of stress is particularly interesting.

The success of the model motivated the present study to provide an analytical framework for understanding the geometrical and mechanical properties of the 30-nm fiber based on the two-angle model. Our first main result is the derivation of a general structural phase diagram of the chromatin fiber as a function of the two basic angles θ and ϕ determined by the nucleosome properties and the linker length b (see below). The various solenoidal, zig-zag and crossed-linker structures—all of which are assumed to have straight linkers—appear as "points" in this phase diagram (see Fig. 4). We find that, within the two-angle model, the position of chromatin fibers at physiological conditions (the "native" fibers) in the phase diagram is surprisingly close to the point in the diagram with the highest density and the maximal accessibility, consistent with excluded-volume restrictions. Changes in bond angles induced by physicochemical changes in the environment lead to predictable changes of the fiber away from this optimal point toward more open structures.

Our second main result is that we can obtain approximate analytical results for the bending stiffness of the two-angle model—and hence for the persistence length—and for the force-extension curve. We find 1) that the persistence length of the fiber should be comparable to or less than that of naked DNA, for a wide range of θ- and ϕ-values; and 2) that the stretching modulus should be so low that there is no longer a pronounced difference between "soft" entropic elasticity (for low forces) and "hard" entropic elasticity (for high forces), in marked contrast with the case of naked DNA. Using the estimated values of θ, ϕ, and b the predicted force-extension curves (with no fitting parameter) are in good agreement with the data found for the stretching of chromatin fibers (Cui and Bustamante, 2000).

The implication of our results is that a swollen 30-nm fiber should be very soft in terms of its elastic properties, over a wide range of values of the angle parameter θ and ϕ, a very reasonable "design feature" in terms of its biological role. This swollen state competes with a more rigid condensed state that appears, as a function of bond angle θ, when we allow for (weak) attractive forces between nucleosomes. The physical properties of the condensed state are beyond the scope of the current paper, but the condensed fiber is expected to be significantly stiffer that the swollen fiber. In general, our results appear to indicate that the "engineering design" of the 30-nm fiber combines high compaction levels with high structural accessibility and flexibility. Independent of the question whether the swollen or the condensed state is realized, modest changes in the control parameter $\pi - \theta$ (the nucleosome entry-exit angle) produce large structural changes.

The paper is organized as follows. In the next section we derive the geometrical properties of the two-angle model and present the general diagram of states. In subsequent sections we apply our results of the two-angle model to interpret the structure of the 30-nm chromatin fiber in terms of simple optimization principles, and derive the elastic properties of the two-angle model and give the bending stiffness and the force-extension relation. In the concluding section we summarize our results and discuss alternative models.

THE TWO-ANGLE MODEL: FOLDED STRUCTURES

General relationships

To address the folding problem of DNA at the level of the 30-nm fiber we need a mathematical description for the different possible folding pathways. At the simplest level, it is assumed that the geometric structure of the 30-nm fiber can be obtained from the intrinsic, single-nucleosome structure. The specific roles of linker elastic energy, nucleosome-nucleosome interaction, preferred binding sites, H1 involvement, etc. will be treated afterward as "corrections" to this basic model. To see how single-nucleosome properties can control the fiber geometry, consider the fact that DNA is wrapped a non-integral number of turns around the nucleosome, e.g., 1¾ times (147 bp) in the case of no H1. This implies that the incoming and outgoing linker chains make an angle θ with respect to each other—the entry-exit angle $\pi - \theta$ is nonzero. In the presence of the histone H1 (or H5) the in- and out-coming linker are in close contact, forming a stem before they diverge (Bednar et al., 1998). Although the precise value of the resulting exit-angle depends on salt concentration, degree of acetylation of the histones, etc., we may nevertheless assume θ to be a quantity that is determined purely at the single-nucleosome level. Next, we define the rotational (dihedral) angle ϕ between the axis of neighboring histone octamers along the necklace (see Fig. 3). Because nucleosomes are rotationally positioned along the DNA, i.e., adsorption of DNA always begins with the minor groove turned in toward the first histone binding site, the angle ϕ is a periodic function of the linker length b, with the 10-bp repeat length of the helical twist of DNA as the period. There is experimental evidence that the linker length shows a preferential quantization involving a set of values that are related by integral multiples of this helical twist (Widom, 1992), i.e., there is a preferred value of ϕ. (Note that the "linker length" b is, strictly speaking, defined here as the distance between two neighboring nucleosomes, cf. Fig. 3.)

If we treat the pair of angles (θ, ϕ), together with the linker length b, as given physical properties (even though in vivo they are likely under biochemical control), then the geometrical structure of the necklace is determined entirely by θ, ϕ, and b. The model only describes linker geometry and does not account for excluded volume effects and other forms of nucleosome-nucleosome interaction; it assumes that the core particles are pointlike ($a = 0$) and that they are located at the joints of the linkers. The model also assumes

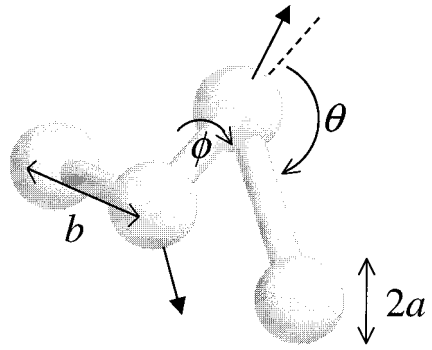

FIGURE 3 Fraction of a two-angle fiber containing four nucleosomes (it is a part of structure "11" in Fig. 4). The two angles are depicted, the deflection angle θ and the rotational angle ϕ, together with the "nucleosome diameter" $2a$ and the "linker length" b. All four are considered to be constant throughout the fiber. The arrows denote the nucleosomal axes, cf. Fig. 1.

that the linkers are straight. It is under dispute whether this last condition holds for the 30-nm fiber at higher salt concentrations, and we will return to this issue later. The (θ, ϕ)-model is similar to the freely rotating chain model encountered in polymer physics literature (see, for instance, Doi and Edwards, 1986). The main difference is that in the present case there is no free rotation around the linker, and so torsion is transmitted (see also Plewa and Witten, 2000).

As shown in Appendix A it is now possible to construct a spiral of radius R and pitch angle γ such that the nucleosomes—but not necessarily the linker chain—are located on this spiral. The nucleosomes are placed along the spiral in such a way that successive nucleosomes have a fixed (Euclidean) distance b from one another. From straightforward geometrical considerations we can derive analytical expressions that relate pitch angle γ and radius R of the solenoid to the pair of angles θ, ϕ, and linker length b. Specifically, the linker length b can be expressed as a function of γ, R, and s_0 (defined as the vertical distance between successive "nucleosomes" along the helical axis), $b = b(\gamma, R, s_0)$, as given by Eq. 32. The corresponding relationships for the angles θ and ϕ, $\theta = \theta(\gamma, R, s_0)$ and $\phi = \phi(\gamma, R, s_0)$, are given by Eqs. 33 and 34. Using these relations, we can construct a catalog of structures.

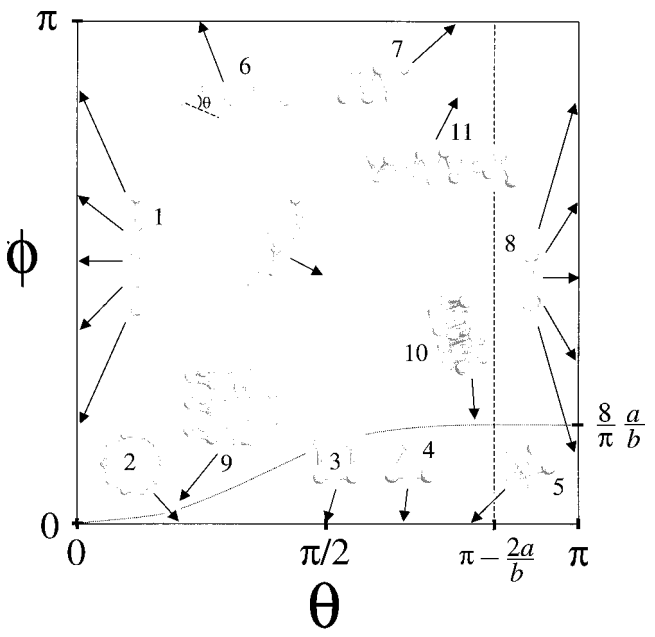

FIGURE 4 Diagram of geometrical states of the two-angle model. Shown are examples of different configurations and their location in the (θ, ϕ)-space (*arrows*). The dashed and dotted curves depict the boundaries to the (θ, ϕ)-values that are forbidden due to excluded volume interaction, one regime (large θ-values) due to "short-range" interaction, the other (small ϕ-values) due to "long-range" interaction (see text for details).

Planar structures

If either one of the angles θ or ϕ assumes the value 0 or π, then the resulting structure is planar, and calculation of the associated geometrical properties is straightforward. Let us start with the case $\phi = 0$. If we also have $\theta = 0$ the fiber forms a straight line (see structure "1" in Fig. 4). For small non-vanishing θ the structure forms a circle of radius $R \simeq b/\theta$. For the special case $\theta = 2\pi/n$, with n an integer, the ring contains n monomers before it repeats itself and we obtain a regular polygon (see "2"). The special case $\theta = \pi/2$ corresponds to the square ("3"). With increasing θ the radius of the circle shrinks and asymptotically approaches the value $b/2$. For $\theta = \pi(n - 1)/n$ with n being an odd integer, one encounters a series of closed star-like polygons with n tips. In particular, $n = 3$ corresponds to the equilateral triangle ("4"), $n = 5$ to the regular pentagram ("5"), etc.

Next we consider the case $\phi = \pi$ and θ arbitrary. This case corresponds to 2D zig-zag-like structures, as shown by "6" and "7" at the top of Fig. 4. The length of a fiber consisting of N monomers is given by

$$L = b \cos(\theta/2)N \tag{1}$$

and the diameter is given by $D = b \sin(\theta/2)$. Note that the length of the fiber increases with decreasing θ.

To complete our discussion of planar structures we mention the remaining cases: $\theta = 0$ with an arbitrary value of ϕ leads to the straight line mentioned earlier ("1"); $\theta = \pi$ and arbitrary ϕ corresponds to linkers that go back and forth between two positions ("8").

Three-dimensional fibers

Solenoids

For small angles, $\theta \ll 1$ and $\phi \ll 1$, we find structures that resemble solenoids where the linkers themselves closely follow a helical path (see "9" in Fig. 4). For these structures one has $\alpha s_0/R \ll 1$, where $\alpha = \cot \gamma$, with γ the pitch angle. To the lowest order in $\alpha s_0/R$ we find $b \simeq s_0\sqrt{1 + \alpha^2}$ (cf. Eq. 32), $\theta \simeq \alpha^2 b/(R(1 + \alpha^2))$ (cf. Eq. 33), and $\phi \simeq \theta/\alpha$ (cf. Eq. 34). From this we can infer several geometrical properties of the fiber as a function of b, θ, and ϕ summarized in Table 1. R denotes the radius of the fiber, L is the length of a fiber consisting of $N + 1$ monomers, λ is its line density N/L, and ρ is the 3D density given by $\rho = \lambda/\pi R^2$, assuming a hexagonal array.

Other geometrical information can be obtained easily. For instance, the vertical distance d between two loops follows from L in Table 1 by setting $N = 2\pi/\theta$ (the number of monomers per turn):

$$d \simeq \frac{2\pi\phi b}{\theta\sqrt{\phi^2 + \theta^2}} \tag{2}$$

Furthermore, the pitch angle γ is given by

$$\cot \gamma \simeq \theta/\phi \tag{3}$$

TABLE 1 Geometrical properties of the two-angle fiber for the three limiting cases: solenoid, fiber with crossed linkers, and twisted zig-zag fiber

	Solenoid ($\phi \ll 1$, $\theta \ll 1$)	Crossed Linkers ($\phi \ll 1$, $\pi - \theta \ll 1$)	Twisted Zig-Zag ($\phi = \pi - \delta$ with $\delta \ll 1$)
R	$\frac{\theta}{\phi^2 + \theta^2} b$	$\frac{b}{2\sin(\theta/2)}\left(1 - \frac{\phi^2}{4}\cot^2(\theta/2)\right)$	$\frac{b}{2}\sin\left(\frac{\theta}{2}\right)\left(1 + \frac{\delta^2}{4}\right)$
L	$\frac{\phi b N}{\sqrt{\phi^2 + \theta^2}}$	$\frac{N\phi b}{2}\cot(\theta/2)$	$b\cos\left(\frac{\theta}{2}\right)N\left(1 - \frac{\delta^2}{8}\tan^2\left(\frac{\theta}{2}\right)\right)$
λ	$\frac{\sqrt{\phi^2 + \theta^2}}{\phi b}$	$\frac{4}{b\phi(\pi - \theta)}$	$\frac{1 + \delta^2\tan^2(\theta/2)/8}{b\cos(\theta/2)}$
ρ	$\frac{(\phi^2 + \theta^2)^{5/2}}{\pi\phi\theta^2 b^3}$	$\frac{16}{\pi\phi(\pi - \theta)b^3}$	$\frac{4}{\pi}\frac{1 + \delta^2(\tan^2(\theta/2)/4 - 1)/2}{b^3\cos(\theta/2)\sin^2(\theta/2)}$

Displayed are the fiber radius R, the length L of a $(N + 1)$-mer, the line density $\lambda = N/L$, and the 3D density $\rho = \lambda/\pi R^2$.

where γ decreases monotonically as the ratio of the angles, θ/ϕ, increases. For $\phi \ll \theta$ one finds $\gamma \simeq \phi/\theta$. In this regime one has a very dense spiral with $d \ll R$. In the opposite limit $\phi \gg \theta$ the pitch angle is very large, namely $\gamma \simeq \pi/2 - \theta/\phi$ and the solenoid has a very open structure with $d \gg R$ (see Notes 3 and 4).

Fibers with crossed linkers

Consider structures where ϕ is still small but where the entry-exit angle θ is large, i.e., $\pi - \theta \ll \pi$. We discussed in the previous section that for $\phi = 0$ one encounters star-shaped polygons that are closed for $\theta = \pi(n - 1)/n$, with n odd. For non-vanishing $\phi \ll 1$ the star-shaped polygons open up in an accordion-like manner. This leads to a three-dimensional fiber with crossed linkers: see "10." It follows from Eqs. 32 and 34 that $s_0^2 \simeq \phi^2 (4R^2 - b^2)/4$ for $\phi \ll 1$. Using this result and Eq. 33, R, L, λ, and ρ can be expressed as a function of b, θ, and ϕ, cf. Table 1.

Assume now that $\theta_n = \pi(n - 1)/n$ so that the projection of the fiber is a closed polygon (this is only strictly true for $\phi = 0$, but it is still a good approximation for $\phi \ll 1$). We can calculate the spacial distance d between nucleosome i and $i + n$ for this case:

$$d \simeq \frac{n\phi b}{2}\cot(\theta/2) \simeq \frac{\pi\phi b}{4}\left(1 + \frac{\pi^2}{12n^2}\right) \qquad (4)$$

Twisted zig-zag structures

Finally, we discuss structures with a rotational angle ϕ close to π, say $\phi = \pi - \delta$ with $\delta \ll 1$. For $\delta = 0$ we recover the 2D zig-zag structure discussed earlier ("6" and "7"). Small non-vanishing values of δ lead to twisted zig-zag structures: see "11." In this case monomer $i + 1$ is located nearly opposite to the ith monomer, but slightly twisted by an angle δ. Monomer $i + 2$ is then on the same side as monomer i but slightly twisted by an angle 2δ, and so on. The geometrical properties are given in Table 1. For $\phi = \pi$, i.e., $\delta = 0$, we recover the result for the planar zig-zag structure.

The fiber is contained within a cylinder of radius R, given in Table 1. The monomers ("histones") are located at the surface, with the linker passing back and forth (approximately) through the middle axis of the cylinder. The monomers n, $n \pm 2$, $n \pm 4$ . . . and the monomers $n \pm 1$, $n \pm 3$, . . . form a double helix that winds around the cylinder. Within each of the two spirals the monomers are not directly linked together, even though monomer i and $i + 2$ can come quite close in space for large values of θ. The pitch angle of the two spirals follows from the positions of monomer 1 and 3; $P_1 = (R, 0, 0)$ and $P_3 \simeq (R, -2R\delta, 2b\cos(\theta/2))$, cf. Eq. 30. Thus $\gamma = -\pi + \Delta\gamma$ with $\Delta\gamma \simeq \delta\tan(\theta/2)/2$.

Structure diagram and excluded volume restriction

We now consider the full range of states in the (θ, ϕ)-space as shown in Fig. 4. Both angles θ and ϕ can each vary over the range 0 to π. At the edges of the diagram where one of the angles assumes an extremal value, the configurations are always planar. On the line $\phi = 0$ we find circles and star-type polygons (that are closed for specific values of θ). The planar zig-zag-structures are located on the line $\phi = \pi$; for $\theta = 0$ we find a straight configuration and for $\phi = \pi$ a "dimer" structure. If we move from the line $\phi = 0$ toward larger values of ϕ the circles and star-like polygons stretch out into the direction perpendicular to their plane, forming a solenoid and a fiber with crossed linkers, respectively. However, if we start at the top of the diagram ($\phi = \pi$) and decrease the value of ϕ, the planar zig-zag structure extends into the third dimension by becoming twisted. If we start with a structure with entry-exit angle $\theta = 0$ and increase the value of this angle, then the structure folds either into a solenoid with large pitch angle for small ϕ-value or into a twisted zig-zag for large values of ϕ. Finally, starting out at the dimer configuration, $\theta = \pi$ leads to an unfolding of the

structure into a fiber with crossed linkers (small ϕ-values) or a twisted zig-zag (large ϕ-values).

If we take into account the excluded volume of the core particles, then certain areas in our phase diagram are forbidden—reminiscent of the familiar Ramachandran plots used in the study of protein folding (Stryer, 1995). For simplicity we assume in the following that the core particles are spherical with a radius a and that their centers are located at the joints of two linkers, cf. Fig. 3. There are two different types of interactions. One is between monomers at position i and $i \pm 2$ (short-range interaction), and leads to the requirement that the entry-angle must be sufficiently small:

$$\theta < 2 \arccos(a/b) \simeq \pi - \frac{2a}{b}, \quad a \ll b \tag{5}$$

This condition excludes a vertical strip at the right side of the diagram, as indicated in Fig. 4 by a dashed line.

There is also a long-range excluded volume interaction that comes into play when the angle ϕ is too small. This is apparent for the case $\phi = 0$, where we find planar structures that run into themselves. Starting with a circular structure we have to increase ϕ above some critical value so that the pitch angle of the resulting solenoid is large enough so that neighboring loops do not interact. This leads to the requirement $d > 2a$ with d given by Eq. 2 (using $\phi \ll \theta$), i.e.,

$$\phi > \frac{1}{\pi}\frac{a}{b}\theta^2 \tag{6}$$

For the large θ-case (fibers with crossed linkers) we find from Eq. 4 the condition

$$\phi > \frac{8}{\pi}\frac{a}{b} \tag{7}$$

The two conditions, Eqs. 6 and 7, shown schematically as a dotted curve in Fig. 4, lead to a forbidden strip in the structure diagram for small values of ϕ.

Figure 4 does not show the interesting "fine-structure" of the boundary of the forbidden strip that is due to commensurate-incommensurate effects. We already noted that there are special θ-values for which the projection of the linkers forms a regular polygonal star ($\theta_n = \pi(n - 1)/n$) or a regular polygon ($\theta'_n = 2\pi/n$) (for small values of ϕ). In these cases the nucleosomes i and $i + n$ "sit" on top of each other. However, for other values of θ, monomers of neighboring loops will be displaced with respect to each other. In this case monomers of one loop might be able to fill in gaps of neighboring loops so that the minimal allowed value of ϕ is smaller than estimated above. We have not explored the interesting mathematical problem of the exact boundary line because this is likely to be sensitive to the exact nucleosome shape. The dotted line in Fig. 4 only represents the upper envelope of the actual curve.

Our discussion of the two-angle model was based on the assumption of a perfectly homogeneous fiber where b, θ, and ϕ are constant throughout the fiber. The effect of randomness in these values on the fiber geometry is discussed in Appendix B.

CHROMATIN AND THE TWO-ANGLE MODEL: OPTIMIZATION OF DESIGN?

Where in the structure diagram is actual chromatin located? The classical solenoid model of Finch and Klug (1976) is found in the small θ, small ϕ section of the diagram (although in their case the linker is bent). Various structures were displayed by Woodcock et al. (1993) in their Fig. 2, namely fibers with $\theta = 150°$ and many different values of ϕ, corresponding to a vertical trajectory on the right-hand side of Fig. 4. Three different configurations with a fixed value of ϕ and different values of θ are displayed in Fig. 3 *c* in another paper by these authors (Bednar et al., 1998).

Our structure diagram accommodates all of these structures and, by itself, does not favor one over another. However, our diagram plus the formulas given above are useful if we invoke the following two criteria to optimize the structure of the 30-nm fiber: 1) maximum compaction and 2) maximum accessibility. The first criterion is obvious: inactive chromatin should be packed as densely as possible because of the very large ratio of DNA length to nucleus size. By the second criterion we mean that a local accessibility mechanism is required for gene transcription.

In order to attain maximum compaction we need structures that lead to high bulk densities ρ (we assume that the 30-nm fibers are packed in parallel, forming a hexagonal lattice). A comparison of the 3D densities of the three different structures given in Table 1 shows that fibers with internal linkers have highest densities ρ, namely

$$\rho \simeq \frac{16}{\pi\phi(\pi - \theta)b^3} \tag{8}$$

In particular, the highest density is achieved for the largest possible value of θ and the smallest possible value of ϕ that is still in accordance with the excluded volume condition. This set of angles is located at the point where the dotted curve and the dashed line in Fig. 4 cross each other. Apparently this also represents the only region in the phase diagram where excluded volume effects are operative on a short-range and a long-range scale at the same time, i.e., nucleosome i is in close contact with nucleosome $i - 2$ and $i + 2$ *and* with nucleosomes farther apart along the contour length of the necklace. This unique set of angles is given by $\theta_{max} \approx 2 \arccos(a/b)$, cf. Eq. 5, and $\phi_{min} \approx (8/\pi)(a/b)$, cf. Eq. 7.

In order to achieve maximum accessibility we look for structures that, for a given entry-exit angle $\pi - \theta$ of a highly compacted structure, achieve the maximum reduction in

nucleosome line density λ for a given small change $\Delta\theta$ of the angle θ. In other words, we look for a maximum of $d\lambda/d\theta$, which we call the "accessibility." Interestingly, the accessibility is maximized at the same unique pair of angles (θ_{max}, ϕ_{min}). This can be seen from its angle dependence for fibers with crossed linkers

$$\frac{d\lambda}{d\theta} \simeq \frac{4}{\phi b(\pi - \theta)^2} \tag{9}$$

We note that this change in λ with θ is achieved by changing the number of monomers per vertical repeat length d. The length d itself is only weakly dependent on n according to Eq. 4.

Before we compare our theoretical formulas with experimental results, we mention that for fibers with crossed linkers there might be another excluded volume interaction, namely between linkers. For these structures the linker connecting the monomers i and $i + 1$ comes closest to the linkers between monomer $i + 2$ and $i + 3$ and the one between $i - 1$ and $i - 2$, as can be seen for the $n = 5$ case, cf. "5" and "10" in Fig. 4. The linkers cross close to the middle of the fiber where the distance between their axes is given by $2(\phi b/2)\cot(\theta/2) \simeq \phi b(\pi - \theta)/2$, cf. Eq. 4. This distance is minimized at (θ_{max}, ϕ_{min}) and has to be larger than the thickness t of the fiber:

$$t < \frac{8}{\pi}\frac{a^2}{b} \tag{10}$$

We now compare the above-given formulas with experimental results. For chicken erythrocyte chromatin one has $\sim b \approx 20$ nm (center-to-center distance of nucleosomes, van Holde and Zlatanova, 1996). Together with $a \approx 5$ nm this leads to $\theta_{max} \approx 151°$, $\phi_{min} \approx 36°$, and $\lambda \approx 6.9$ nucleosomes per 11 nm (cf. Eqs. 5, 7, and 8). Furthermore, the condition on the linker thickness is given by $t < 3.2$ nm and is fulfilled, because $t = 2$ nm for DNA. The theoretically derived values can now be compared with the ones reported by Bednar et al. for chicken erythrocyte chromatin fibers (Bednar et al., 1998). From their Table 1 we find that for an ionic strength of 80 mM (which is close to the physiological value) $\theta \approx 145°$ and $\lambda = 5.9$ nucleosomes per 11 nm. Furthermore, electron cryotomography-constructed stereo pair images of an oligonucleosome (cf. Fig. 3 *b* in Bednar et al., 1998) indicate that the chromatin fiber might indeed have the structure of a fiber with crossed linkers, with $n \approx 5$; this would correspond to $\theta = \pi(n - 1)/n \approx 144°$.

Information concerning the preferred value for ϕ may be obtainable from the measured statistical distribution of the nucleosome repeat lengths. This distribution shows statistically preferred linker lengths equal to $10k + 1$ bp with k a positive integer (Widom, 1992) which, in turn, indicates that the rotation angle ϕ corresponds to a change in helical pitch associated with 1 bp, i.e., $360°/10 = 36°$. This value coincides with ϕ_{min}, the value that we estimated for maximum compaction (see Note 5).

The second feature, the local accessibility, can be monitored in vitro by changing the salt concentration. Bednar et al. report, for example, that θ decreases with decreasing ionic strength, namely $\theta \approx 145°$ at 80 mM, $\theta \approx 135°$ at 15 mM, and $\theta \approx 95°$ at 5 mM (Bednar et al., 1998). In the biochemical context the change of θ is accomplished by other mechanisms, especially by the depletion of linker histones and the acetylation of core histone tails (cf., for instance, van Holde and Zlatanova, 1996), both of which are operative in transcriptionally active regions of chromatin. These mechanisms lead effectively to a decrease of θ.

As pointed out below Eq. 9, the decrease of θ is accompanied by a decrease of the line-density $\lambda = n/d$ of nucleosomes at an essentially fixed value of d. In other words, the number of vertices of the projected polygon decreases significantly with decreasing θ because $\theta_n = \pi(1 - 1/n)$. In that respect the effect of reducing θ below the optimal packing value might be best viewed as an "untwisting" of the 30-nm fiber. Using the experimentally determined values of θ we find from Table 1 that the density (the number of nucleosomes per 11 nm) is given by $\lambda \approx 6.8$ for $\theta \approx 145°$, $\lambda \approx 4.5$ for $\theta \approx 135°$, and $\lambda \approx 2.3$ for $\theta \approx 95°$, slightly higher than the experimental values $\lambda \approx 6.0$, $\lambda \approx 3.2$, and $\lambda \approx 1.5$ (Bednar et al., 1998). Furthermore, the number of polygonal vertices $n = \pi/(\pi - \theta)$ decreases as follows: $n \approx 5.1$ for $\theta \approx 145°$, $n \approx 4.0$ for $\theta \approx 135°$, and $n \approx 2.1$ for $\theta \approx 95°$, consistent with the stereo pair images by Bednar et al., suggesting $n \approx 5$ at an ionic strength of 80 mM and $n \approx 3$ at 5 mM (cf. Figs. 3 *a* and *b* in Bednar et al., 1998).

We close this section with a cautionary remark. The 3D density and the line density of the fiber cannot only be changed by changing θ or ϕ, but also by changing the linker length (in multiples of 10 bp). A variation in b changes the location of the point (θ_{max}, ϕ_{min}) in the diagram of geometrical states, and thus the values of the maximum 3D and line densities that can be achieved, namely

$$\rho_{max} \simeq \frac{16}{\pi\phi_{min}(\pi - \theta_{max})b^3} \simeq \frac{1}{a^2 b} \tag{11}$$

and

$$\lambda_{max} \simeq \frac{4}{b\phi_{min}(\pi - \theta_{max})} \simeq \frac{\pi}{4}\frac{b}{a^2} \tag{12}$$

This shows that fibers with smaller values of b can achieve higher 3D densities but have a smaller maximal line density (and accessibility $d\lambda/d\theta \propto b^2$). From this one might infer that active cells should have larger nucleosome repeat lengths in order to maximize the accessibility to their genetic material. An overview on nucleosome repeat lengths in different organisms and tissues is given in Table 7-1 of van Holde's book (van Holde, 1989). The data shown there

do not follow this rule, unfortunately. In fact, very active cells like yeast cells and neuronal cells have, in general, short nucleosome repeat lengths, while inactive ones like sperm cells have large ones. This shows that the optimization principle of high density has to be used with caution.

STRETCHING AND COMPRESSION OF TWO-ANGLE FIBERS

The (θ, ϕ, b) model developed so far is purely geometrical. Could it be useful as well for predicting physical properties of the 30-nm fiber? The response of the 30-nm fiber to elastic stress will be the focus of this section. The elastic stress can either be of external or of internal origin. External stresses are exerted on the chromatin during the cell cycle when the mitotic spindle separates chromosome pairs. The 30-nm fiber should be both highly flexible and extensible to survive these stresses. The in vitro experiments by Cui and Bustamante demonstrated that the 30-nm fiber is indeed very "soft" (Cui and Bustamante, 2000).

The 30-nm fiber is also exposed to internal stresses. Attractive or repulsive forces between the nucleosomes will deform the linkers connecting the nucleosomes. For instance, electrostatic interactions, either repulsive (due to the net charge of the nucleosome core particles) or attractive (bridging via the lysine-rich core histone tails; Luger et al., 1997) could lead to considerable structural adjustments of the (θ, ϕ, b) model.

In this section we will derive an analytical description of the force extension curve of the (θ, ϕ, b) model in order to predict the elastic properties of the different structures obtained in the previous section. Using the particular values of θ and ϕ that are observed experimentally (Bednar et al., 1998; Widom, 1992), we can reproduce rather well the measured force-extension curve of Cui and Bustamante and the numerical results of Katritch et al. that were based on a variant of the (θ, ϕ, b) model (see below).

Before considering the elastic properties of the (θ, ϕ, b) model, it is helpful to briefly recall some results concerning the large-scale elasticity of the DNA itself (Cluzel et al., 1996; Marko, 1998). The measured force-extension curve of naked DNA breaks up into two highly distinct regimes: the "entropic" and "enthalpic" elastic regimes. For very low tension f ($\lesssim$1 pN), the restoring force is provided by "entropic elasticity" (de Gennes, 1979). In the absence of any force applied to its ends, the DNA's rms end-to-end distance (chain length, L) is small compared to its contour length (L_0) and the chain enjoys a large degree of conformational disorder. Stretching DNA reduces its entropy and increases the free energy. The corresponding force f increases linearly with the extension L:

$$f \simeq \frac{3k_BT}{A_{DNA}}\frac{L}{L_0}, \quad L \ll L_0 \tag{13}$$

The length A_{DNA} is known as the "thermal persistence length" of DNA and is of the order 50 nm (Hagerman, 1988).

For higher forces ($f \gtrsim 10$ pN), the end-to-end distance L is close to L_0 and the elastic restoring force is due to distortion of the internal structure of DNA. In this regime, the force extension curve can be approximated by

$$f \simeq k_BT\gamma_{DNA}\frac{L - L_0}{L_0}, \quad L \gtrsim L_0 \tag{14}$$

We will call $\gamma = (\partial f/\partial L)L_0/k_BT$ the "stretching modulus." γ_{DNA} is $\sim$300 nm^{-1} (Cluzel et al., 1996; Smith et al., 1996), i.e., almost four orders of magnitude larger than the corresponding value $3/A_{DNA}$ obtained from Eq. 13.

Bending and twisting of linker

To calculate the stretch modulus of the (θ, ϕ, b) model, each linker is modeled as a wormlike chain (WLC) of fixed length b (see Schlick, 1995 for a review of the WLC). We denote the geometrical configuration of the kth linker (k = 1, 2, 3, . . .) by $\mathbf{r}_k(s)$, with s being the arclength, $0 \le s \le b$. The elastic energy of the wormlike linker is given by the sum of the bending and the torsional energies:

$$E_k = \tfrac{1}{2}\int_0^b ds\left\{\kappa\left(\frac{1}{R_k(s)}\right)^2 + C\left(\frac{d\eta_k(s)}{ds}\right)^2\right\} \tag{15}$$

Here κ is the bending stiffness which is related to the persistence length A_{DNA} of (linker) DNA by $\kappa = k_BT\,A_{DNA}$. Furthermore, $1/R_k(s) = |d^2\mathbf{r}_k(s)/ds^2|$ denotes the curvature of the kth linker at the point s along its contour. The torsional angle of the linker is $\eta_k(s)$ and the torsional stiffness is C. The positions $\mathbf{r}_k(0)$ and $\mathbf{r}_k(b)$ of the two termini of the kth linker coincide with the termini of the neighboring linkers, i.e., $\mathbf{r}_{k-1}(b) = \mathbf{r}_k(0)$ and $\mathbf{r}_k(b) = \mathbf{r}_{k+1}(0)$. Furthermore, we assume that the entry-exit angles have the fixed value $\pi - \theta$ independent of the bending and twisting of the linkers. This means that the unit tangents fulfil the condition $\cos(\theta) = \mathbf{t}_k(b) \cdot \mathbf{t}_{k+1}(0)$, with $\mathbf{t}_k(s) = d\mathbf{r}_k(s)/ds$.

Enthalpic elasticity

We first study the stretching of the planar zig-zag pattern ($\phi = \pi$, θ arbitrary). The undeformed zig-zag fiber is depicted in Fig. 5 *A*. In order to give a more accurate description of the mechanical properties of the fiber, we assume that the nucleosome core particles are not located at the sites where two linkers come together, but rather slightly displaced, forming a stem configuration as shown in Fig. 5 *A*. This is the geometry obtained from the electron cryomicrographs of Bednar et al. (1998) and it is the same geometry that was adopted in the computer simulations of

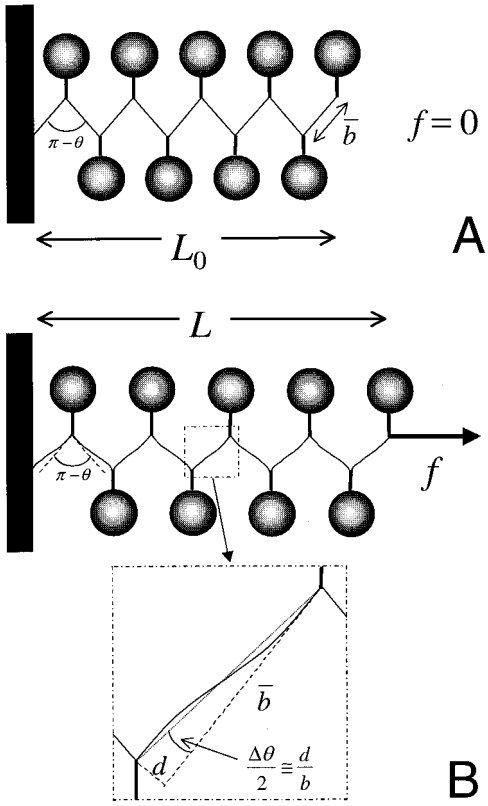

FIGURE 5 Stretching of a zig-zag chain. (*A*) The unperturbed chain ($F = 0$) has a total length L_0 and straight linkers. (*B*) The same fiber under tension $F > 0$. The fiber is stretched to an end-to-end distance $L > L_0$ by bending of the linkers. The linkers are bent in such a way that the entry-exit angles at the individual nucleosomes remain unchanged.

fiber stretching (Katritch et al., 2000). In the following we denote the actual linker length by $\bar{b}$ in order to distinguish it from b, the distance between neighboring nucleosomes. For symmetry reasons, there is no torque on the structure, so that $d\eta_k/ds \equiv 0$. The stretching of the fiber is achieved by a bending of the linkers with the entry-exit-angle θ remaining constant (cf. Fig. 5 *B*). This leads to a deformation where the tangent vectors $\mathbf{t}_k(0)$ and $\mathbf{t}_k(\bar{b})$ remain parallel but undergo lateral displacement. We assume a small deformation of the linker with displacement $u(s)$ from the straight configuration small compared to $\bar{b}$. (Because $u(s)$ is the same for all the linkers, we drop the index k from here on.)

From the minimization of E_k, Eq. 15, we obtain the Euler-Lagrange equation $d^4u/ds^4 = 0$. The boundary conditions that must be obeyed by the solutions are $u(0) = u'(0) = u'(\bar{b}) = 0$ and $u(\bar{b}) = d$, where d describes the displacement of the bead vertical to the original straight linker (we assume $d \ll \bar{b}$ here and neglect terms of the order $(d/\bar{b})^2$). It follows that the deformation profile is given by $u(s) = -2ds^3/\bar{b}^3 + 3ds^2/\bar{b}^2$. The associated bending energy is $E = 6\kappa d^2/\bar{b}^3$ (per linker). The deformation translates into an effective change in the deflection angle from θ to $\theta - \Delta\theta$ where $\Delta\theta/2 = d/\bar{b}$; see Fig. 5 *B*. The energy of a fiber with N linkers as a function of $\Delta\theta$ is thus given by $E = (3/2)(\kappa/\bar{b})(\Delta\theta)^2 N$.

The change in θ produces a change in the overall length of the fiber. We find from Eq. 1:

$$L = \bar{b}N\cos\left(\frac{\theta-\Delta\theta}{2}\right)$$

$$\simeq L_0 + \bar{b}N\sin(\theta/2)\Delta\theta/2, \quad \Delta\theta \ll 1 (\leftrightarrow d \ll \bar{b}) \tag{16}$$

where L_0 is the contour length of the unperturbed fiber, Eq. 1. The energy can be rewritten in terms of the extension $\Delta L = L - L_0$. The restoring force follows then from $f = dE/dL$:

$$f \simeq \frac{12}{N\sin^2(\theta/2)}\frac{\kappa}{\bar{b}^3}\Delta L \tag{17}$$

The associated stretching modulus (defined as in Eq. 14) follows from Eqs. 1 and 17:

$$\gamma_{\text{fiber}}(\theta) \simeq \frac{12A_{\text{DNA}}}{\bar{b}^2}\frac{\cos(\theta/2)}{\sin^2(\theta/2)} \tag{18}$$

We next consider the deformation of fibers with crossed linkers ($\phi \ll 1$, θ large). When such a fiber is stretched, linkers will be twisted and bent. Interestingly, a fiber with a high bending stiffness ($\kappa \to \infty$) can still be stretched just by twisting the linkers. When one applies a tension to such a fiber each linker is twisted and the rotational angle changes by $\Delta\phi$ from one linker to the next, i.e., $d\eta/ds = \Delta\phi/\bar{b}$. The twist is distributed homogeneously along the linker since $d^2\eta/ds^2 = 0$, which follows from minimization of E_k in Eq. 15. The energy per linker is given by $E = (C/2)(\Delta\phi^2/\bar{b})$. The twist of the linkers changes the length of the fiber, and using L from Table 1 it is straightforward to calculate the force as a function of the relative extension:

$$f \simeq \frac{4C}{\cot^2(\theta/2)\bar{b}^3N}\Delta L \tag{19}$$

In the opposite limit of linkers with extremely high torsional stiffness ($C \to \infty$), the force-extension curve can be mapped onto the planar zig-zag case, described above, by replacing $\pi - \theta$ by $\tilde{\phi} \simeq \phi\cot(\theta/2)$, the "effective" angle between two consecutive linkers as seen from the "side" of the fiber. (This follows from $\tilde{\phi} \simeq 2\Delta l/\bar{b}$, where Δl is the difference in the longitudinal position of bead i and $i + 1$; $\Delta l = (\phi\bar{b}/2)\cot(\theta/2)$). Using Eq. 17 we find

$$f \simeq \frac{12\kappa}{\bar{b}^3N\cos^2(\tilde{\phi}/2)}\Delta L \tag{20}$$

We can now define as before the two stretching moduli γ_{twist} and γ_{bend} using Eqs. 19 and 20 together with Eq. 4. If we allow both twist and bend, then the two "spring con-

stants" act "in series": $\gamma_{\text{fiber}}^{-1} = \gamma_{\text{twist}}^{-1} + \gamma_{\text{bend}}^{-1}$. We obtain for the stretching constant of the fiber ($\phi \ll 1$, θ large)

$$\gamma_{\text{fiber}}(\theta, \phi) = \gamma_{\text{bend}}\left(1 + \frac{\gamma_{\text{bend}}}{\gamma_{\text{twist}}}\right)^{-1} = \frac{6A_{\text{DNA}}}{\bar{b}^2}\frac{\tilde{\phi}}{\cos^2\left(\frac{\tilde{\phi}}{2}\right)}\left[1 + \frac{3\cot^2\left(\frac{\theta}{2}\right)}{\cos^2\left(\frac{\tilde{\phi}}{2}\right)}\frac{\kappa}{C}\right]^{-1} \quad (21)$$

For large n (with n defined as $n = \pi/(\pi - \theta)$) the twisting contribution can be neglected because then $\gamma_{\text{bend}}/\gamma_{\text{twist}} \approx (3/4)(\pi/n)^2(\kappa/C)$. For DNA $C \simeq k_B T \times 750$ Å $\gtrsim \kappa$ (Klenin et al., 1989; Crothers et al., 1992) so that $\gamma_{\text{bend}} \ll \gamma_{\text{twist}}$ for $n \gtrsim 5$. In this case one has $\gamma_{\text{fiber}} \simeq \gamma_{\text{bend}}$ and Eq. 20 applies.

Entropic elasticity

Just as for naked DNA, the entropic contribution to the elasticity dominates for weak forces ($L \ll L_0$). The restoring force is again of the form

$$f = \frac{3k_B T}{A_{\text{fiber}}}\frac{L}{L_0} \quad (22)$$

with A_{fiber} the persistence length of the fiber. This persistence length is calculated in Appendix C. For the case of the crossed-linker fiber we find

$$A_{\text{fiber}} \approx A_{\text{DNA}}\frac{\phi}{2}\cot(\theta/2) \quad (23)$$

For values of θ and ϕ appropriate for the crossed-linker structure, A_{fiber} is somewhat less than A_{DNA} (of the order of 50 nm). This surprising conclusion is related to the fact that a large amount of DNA material is stored in the fiber per unit length. The 30-nm fiber is thus indeed highly flexible.

Our calculation of the stretching properties of the two-angle model predicts an important difference between the stretching behavior of DNA and that of the 30-nm fiber. The enthalpic stretching modulus of a chromatin fiber is of the order $A_{\text{DNA}}/\bar{b}^2$ (see Eqs. 18 and 21), which is $\sim 0.3\ \text{nm}^{-1}$ for 40-bp linkers ($\bar{b} = 40 \times 0.34$ nm $\simeq 14$ nm). This is only an order of magnitude larger than the entropic stretching modulus $1/A_{\text{fiber}} \simeq 0.03\ \text{nm}^{-1}$. In other words, because of the low value of γ_{fiber} and because $A_{\text{fiber}} \approx A_{\text{DNA}}$, there is no longer a very clear distinction between entropic and enthalpic behavior as it is observed for naked DNA. In conclusion, the 30-nm fiber shows soft elasticity under stretching due to bending and twisting of the linkers.

Internucleosomal attraction

The effect of attractive interaction between nucleosomes is to cause a compression of the 30-nm fiber. Phase behavior studies of linker-free nucleosome solutions, i.e., solutions of disconnected nucleosomes (Livolant and Leforestier, 2000; cf. also Fraden and Kamien, 2000) indicate that nucleosome core particles spontaneously form fiber-like columnar structures, presumably due to attractive nucleosome-nucleosome interaction. Attractive nucleosome interaction could be mediated, for instance, by the lysine-rich core histone tails (Luger et al., 1997), as mentioned above.

It is important to distinguish these condensed fibers from the swollen solenoid-, zig-zag-, and crossed-linker structures predicted by the (θ, ϕ, b)-model. The dominant energy of the condensed structures is the nucleosome attractive interaction, while the "swollen" structures are dominated by linker elasticity. In this section we will discuss the competition between swollen and condensed phases for a simple case.

For simplicity, we model the fiber as a planar zig-zag structure with elastic linkers and assume in addition a short-range interaction between nucleosomes. This interaction, denoted by U_{inter}, is assumed to be a short-range attraction, of strength $-U_{\text{min}}$, that acts only when the nucleosomes are in close contact, i.e., at a distance $x \approx 2a$ of the order of the hardcore diameter. For a given nucleosome, say the ith, the closest nucleosomes in space are number $i + 2$ and $i - 2$, as discussed previously. We will disregard the interaction between other pairs. The elastic interaction U_{el} follows directly from Eq. 17 with $N = 2$:

$$U_{\text{bend}}(x) = \frac{3}{\sin^2(\theta/2)}\frac{\kappa}{\bar{b}^3}(x - x_0)^2 = \frac{K}{2}(x - x_0)^2 \quad (24)$$

where $x_0 = 2\bar{b}\cos(\theta/2)$ denotes the distance between nucleosome i and $i + 2$ for straight linkers (cf. Eq. 1). The total internucleosomal $U(x)$ equals $U_{\text{inter}}(x) + U_{\text{bend}}(x)$.

Fig. 6 *A* shows $U(x)$ for different values of θ. We assume for simplicity that the interaction energy U_{inter} remains unchanged. Curve "1" in Fig. 6 *A* shows $U(x)$ for a small value of θ where the global minimum of $U(x)$ is located at $x = x_0$, denoted by "S" (swollen state). Curve "2" corresponds to an intermediate value of θ at which the minima at "S" and "C" have the same value. For this value of θ, $\theta = \theta_c$, the energy minimum shifts from "S" to a new minimum, representing the condensed state "C." The change in θ produced a structural transition from a swollen state to a condensed state. Finally, curve "3" depicts $U(x)$ for a deflection angle $\theta > \theta_c$ with the minimum at "C." The critical angle for the "S" to "C" transition can be determined by comparing the bending energy at close contact, $U_{\text{bend}}(2a)$, and the strength U_{min} of the short range attraction. Equating

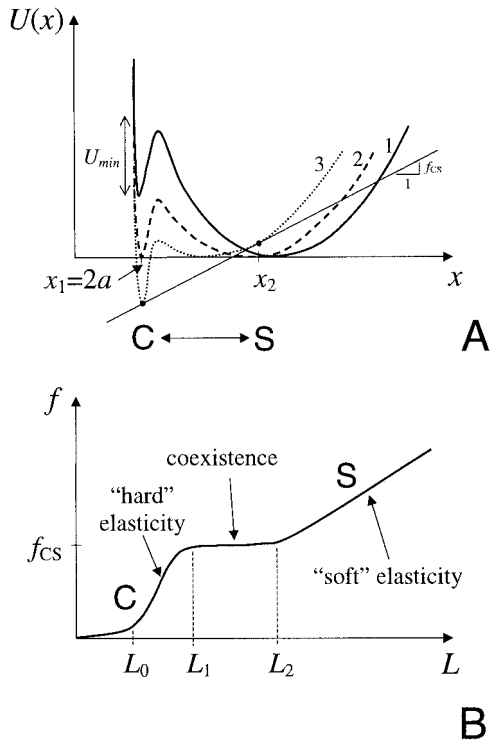

FIGURE 6 (*A*) Internucleosomal interaction potential U between nucleosome i and $i + 2$ as a function of distance x. In addition to the elastic contribution there is a short-range attraction for nucleosomes at close contact, $x = 2a$. The different curves correspond to different values of the angle θ. Curve "1" has the global minimum at large x (swollen state "S"), whereas curve "3" has the minimum for nucleosomes in close contact (condensed state "C"). Curve "2" corresponds to the transition point. Also depicted is the common tangent for curve "2". Its slope corresponds to the critical stretching force f_{CS} at which nucleosomes are transferred from the condensed to the stretched state. (*B*) Force-extension curve of a condensed fiber (say, the fiber with the interaction potential "3"). For extensions L with $L_1 < L < L_2$ one finds a coexistence plateau with the restoring force f_{CS} (see text for details).

both leads to the following condition for θ_c:

$$\cos(\theta_c/2) - \sqrt{\frac{\bar{b}(U_{min}/kT)}{6A_{DNA}}}\sin(\theta_c/2) = \frac{a}{\bar{b}} \qquad (25)$$

In the swollen state the elastic properties are those discussed in the previous section. In the condensed state, the elastic properties are determined by the detailed form of the nucleosome interaction potential.

If the condensed state has a lower free energy, i.e., if $\theta > \theta_c$, then an external stretching force f can induce a transition from the condensed to the swollen state. The transition point f_{CS} follows from a "common-tangent" construction. The conditions are $U'(x_1) = U'(x_2) = f_{CS}$ and $(U(x_2) - U(x_1))/(x_2 - x_1) = f_{CS}$ (cf. Fig. 6 *A*). The first pair of conditions leads to $x_1 = 2a$, $x_2 = x_0 + f_{CS}/K$. The last condition leads to

$$f_{CS} = \sqrt{2KU_{min}} - K(x_0 - 2a) \qquad (26)$$

The corresponding force-extension curve has a "coexistence plateau" (cf. Fig. 6 *B*). If the imposed end-to-end distance is smaller than L_0 (the contour length of the condensed fiber) then the restoring force is entropic. For $L_0 < L < L_1$ the force rises sharply with increasing L. This "hard elasticity" is governed by the nucleosomal interaction potential U_{inter}. Then at $L = L_1$ the coexistence plateau is reached. Between $L = L_1$ and $L = L_2$ parts of the fiber are in the "S" state and parts are in the "C" state. For larger extensions, $L > L_2$, the fiber shows soft elasticity due to the bending (and twisting) of the linkers as discussed in the previous section.

Stretching chromatin

We now compare the results of the previous two sections with the force extension curves found in recent experiments (Cui and Bustamante, 2000).

Low ionic strength

We start with the force-extension profile measured at low ionic strength (5 mM), cf. Fig. 2 in Cui and Bustamante. As discussed above, at low ionic strength the chromatin fiber constitutes a swollen fiber with crossed linkers. The nucleosomes are far apart and we assume that there is no direct interaction between nucleosomes. The resulting force-extension profile is expected to show a crossover between an entropic elasticity (cf. Eq. 22) and a soft enthalpic elasticity with a stretching modulus given by Eq. 21:

$$f \simeq \begin{cases} \dfrac{6k_BT}{l_p\bar{b}\tilde{\phi}N}L & \text{for } L \ll L_0 \\ \dfrac{2k_BT\gamma_{fiber}}{\tilde{\phi}\bar{b}N}(L - L_0) + \dfrac{3k_BT}{l_p} & \text{for } L \gg L_0 \end{cases} \qquad (27)$$

with $L_0 \simeq (\tilde{\phi}/2)\bar{b}N$ (cf. Table 1).

Cui and Bustamante estimate the number of nucleosomes in their fibers to be $N \approx 280$. From the formula for L in Table 1, we would estimate the length of the fiber to be $L_0 \approx 1.0\ \mu$m using the values $\theta = 95°$ (Bednar et al., 1998), $\phi = 36°$ (Widom, 1992), and $\bar{b} = 40$ bp $= 40 \times 0.34$ nm $= 1.4 \times 10^{-8}$ m. The linker length is estimated from the nucleosome repeat length of ~210 bp (cf. Table 7-1F in van Holde, 1989) minus ~170 bp that are associated with the core and linker histones (cf. page 268 in van Holde, 1989). Using the moduli for DNA (Hagerman, 1988), $\kappa = k_BT \times 50$ nm $= 2 \times 10^{-16}$ pN m^2, $C = k_BT \times 75$ nm $= 3 \times 10^{-16}$ pN m^2, and $l_p = 30$ nm for the persistence length of the fiber (cf. Appendix C), we find from Eq. 27 the following force-extension relation (force in piconewtons, extension in microns):

$$f \simeq \begin{cases} 0.35 \times L & \text{for } L \ll 1.1 \\ 1.2 \times (L - 1.0) + 0.4 & \text{for } L \gg 1.1 \end{cases} \qquad (28)$$

The agreement with the experimental curve at low ionic strength (5 mM NaCl) is reasonable (cf. Fig. 2, *a* and *b* in Cui and Bustamante, 2000). More explicitly, for forces up to 5 pN and extensions up to $\approx 2\ \mu$m there are two distinctive regimes: for small extensions, $L \lesssim 1\ \mu$m, the force increases only slightly with tension, namely roughly as $f \approx 0.5 \times L$. Then for $L \gtrsim 1\ \mu$m the measured force increases much faster and shows the following linear dependence: $f \approx 7 \times L$ (Fig. 2 *A*) or $f \approx 5 \times L$ (Fig. 2 *B*). The different slopes in this regime are a result of a slight hysteresis: the relaxation curve has a smaller slope after the fiber has been stretched to an end-to-end distance of 2.5 μm (Fig. 2 *B*) than for the case of a much smaller stretching cycle (up to 1.8 μm, Fig. 2 *A* in Cui and Bustamante, 2000); the hysteresis disappears for a smaller rate of extension or contraction, and might be a result of nucleosome-nucleosome interaction or of modifications of the fiber close to the entry-exit point of the linkers at higher tension. We also mention that for forces beyond ≈5 pN the (relaxation) curve shows an increasing slope, probably due to nonlinear effects not accounted for in the current study (see Note 6).

The calculated forces are smaller than the measured ones (roughly by a factor of 4), for several reasons. First, the (mean) values of θ, ϕ, and $\bar{b}$ (and thus N) are only roughly known. Second, the value of θ we used (95°) is not large enough compared to π for the above-given theoretical formulas to hold accurately. However, as a check of our analytical approximations, we compared our results with the computer simulations by Katritch et al. (2000) where θ, ϕ, and $\bar{b}$ are variable. This comparison is given in Appendix D, where we show that there is good agreement indicating that our analytical approximations were in fact reasonable.

High ionic strength

For 40 mM NaCl or higher ionic strength the chromatin fiber is much denser and nucleosomes approach each other closely. Attractive short-range forces and the increase of θ associated with higher ionic strength should favor the condensed phase. A plateau indeed appears at 5 pN in the force-extension plot (cf. Fig. 4 in Cui and Bustamante, 2000). From the extent of the plateau, 0.6 μm, its height, 5 pN, and the number of nucleosomes in the stretched fiber, ≈280, it was estimated that there is an attractive interaction energy of ~3 kT per nucleosome (Cui and Bustamante, 2000).

We now can use Eq. 26 to independently estimate the strength of the nucleosomal attraction from the value of the critical force alone. We find:

$$U_{\min} = \frac{(f_{CS} + K(x_0 - 2a))^2}{2K} \tag{29}$$

If we neglect the second term in the bracket, we find $U_{\min} \approx f^2/(2K) \approx 6$ kT (assuming $\theta = 140°$), close to the value 3 kT estimated directly from the force-extension diagram (Cui and Bustamante, 2000) and also in accordance with the computer simulation of Katritch et al. who obtained an internucleosomal short-range attraction of order 2 kT (Katritch et al., 2000).

Using $U_{\min} = 3$ kT we can estimate the critical value $\theta = \theta_c$ at which the condensed and the swollen chromatin fiber should coexist. We find numerically from Eq. 25 that $\theta_c \approx 100°$ (using $a = 5$ nm and $\bar{b} = 14$ nm). This value is lower than the one that can be inferred from experiments. At 15 mM NaCl ($\theta \approx 135°$) the fiber appears to be decondensed, as indicated by stretching experiments and from electron cryomicrographs. This fact, and the appearance of a plateau in the force extension curve at 40 mM salt (where $\theta \approx 140°$) indicates that one should expect $135° \lesssim \theta_c \lesssim 140°$ (cf. Bednar et al., 1998). It should be recalled, however, that our model for the attractive interaction is highly oversimplified.

CONCLUSIONS

The present analytical study of the (θ, ϕ, b) model first of all shows that this model can account for the measured force-extension curve of the 30-nm fiber in the low-salt regime with, in effect, no fitting parameters (because θ, ϕ, and b can be estimated experimentally and the elastic moduli characterizing naked DNA are known). Since the (θ, ϕ, b) model also accounts for the observed low-salt structure of the 30-nm fiber ("crossed linkers"), there seems to be good evidence that this model is at least the proper description in the low-salt regime.

We have been able to compute the structural and elastic properties over a wide range of (θ, ϕ)-values. We suggest that the native chromatin fiber might be a particular realization of this rich array of structures, namely the one that simultaneously maximizes compaction and accessibility, consistent with the restriction of excluded volume between nucleosomes.

Confirmation that a certain optimization principle is in fact operative for biomolecules is usually a difficult issue. We already saw that, at best, the principle is incomplete because the linker-length b evidently is not determined by the conditions of maximum compaction and accessibility. One possibility may be to explore the fine structure of the dotted curve in Fig. 4, the lower bound of ϕ as a function of θ. This is expected to have an "irregular" shape due to commensurate-incommensurate effects and it may be possible to associate a discrete geometrical structure (e.g., a particular index n for the polygonal star projection) with maximum compaction and accessibility. Such a study would require, however, a better description of the structure of individual nucleosomes and extensive numerical work.

How confident can we be that the (θ, ϕ, b) model is appropriate as well in the biologically relevant regime of physiological salt concentrations? We had to include a weak attractive nucleosome interaction to explain the coexistence

in the force-extension curve. If the fitted value for the attractive potential ($U_{\min}$) is used in Eq. 25 we obtain a reasonable estimate for the critical angle θ_c for the "S" to "C" transition (but with a significant error).

A completely different approach would be that the high-salt regime is controlled not by a balance between soft elasticity and weak attraction, but completely by nucleosome-nucleosome attraction forces (plus short-range repulsion). As shown by the work of Livolant and Leforestier (2000), nucleosome attraction indeed can produce discoidal fiber structures (formed by linker-free core particles) all by itself. If the interaction energy is strong enough, then the linkers would be strongly bent in the condensed state. The (θ, ϕ, b) model would not be a valid description anymore. The effect of tension could be to produce a sequence of different condensed structures. Only at high tension, when the internucleosomal contacts are broken, one recovers the soft-elasticity regime, described well by the (θ, ϕ, b)-model. Which of the two approaches is valid is an issue that must be determined experimentally.

Interesting questions for "chromatin physics" in the future may focus on dynamical issues. Suppose that θ is locally increased, e.g., by acetylation of core histone tails; how long does it take for the accessibility to increase sufficiently? How important are nucleosome mobility (Schiessel et al., 2001) and nucleosome "evaporation" (Marko and Siggia, 1997) for the swelling dynamics of chromatin?

NOTES

1. Experiments on dinucleosomes (two nucleosomes connected by one linker) have been performed to check if the nucleosomes "collapse" upon an increase in ionic strength. A collapse would only occur if the linker bends, and an observation of this phenomenon would support the solenoid model. The experiments by Yao et al. (1990) and more recent experiments by Butler and Thomas (1998) indeed reported a bending of the linkers but do not agree with experiments by Bednar et al. (1995) and by others that did not find any evidence for a collapse. Critical discussions of these and other experiments on dinucleosomes are available (van Holde and Zlatanova, 1996; Widom, 1998).

2. Marko and Siggia (1997) had in fact proposed an elastic model that predicted a coexistence regime in the force-extension curve, with nucleosomes "evaporating" from the fiber at higher force levels of the order of 2 pN, which would lead to extensive irreversibility in the force-extension curve. Although irreversibility is encountered at high force levels, as mentioned, the 5-pN plateau is reversible, indicating that there was no nucleosomal loss.

3. We note that such an open structure could in principle collapse into a very dense fiber like the solenoidal model proposed by Klug (cf. Fig. 2 *A*) if we would allow the linkers to bend. As mentioned before, it is still a matter of controversy if such linker bending takes place in chromatin. We will stick in this study to the assumption of straight linkers.

4. We mention that in the limit $\phi \to 0$ we recover the planar circle with radius $R \simeq b/\theta$, cf. Table 1.

5. The statistical uncertainty around the expectation values for the nucleosome repeat length is sufficiently large to make our estimate for ϕ less reliable.

6. Our calculation is based on the assumption of small deformations. For the zig-zag case this requires $d \ll \bar{b}$, i.e., $\Delta\theta \ll 1$, cf. Fig. 5 *B*. Using Eqs. 16 and 17 this condition translates into the requirement that the tension f is smaller than $6\kappa/(\bar{b}^2 \sin(\theta/2))$. For fibers with internal linkers the condition is $\Delta\tilde{\phi} \ll 1$, leading to $f \ll 6\kappa/(\bar{b}^2 \cos^2(\tilde{\phi}/2))$. Thus, in both cases a good estimate for the range of forces where the linear approximation holds is given by $f < 6\kappa/\bar{b}^2$. For the chromatin fiber under consideration we find $6\kappa/\bar{b}^2 \simeq 6$ pN.

APPENDIX A: THE MASTER SOLENOID

For any given set of angles (θ, ϕ) there is a solenoid so that the successive monomers of the fiber structure lie successively on this helical path. (There are actually many such solutions, but we are interested in the one with the largest pitch angle γ.) We parametrize the solenoid as follows

$$\mathbf{r}(s) = \begin{pmatrix} R\cos(\alpha s/R) \\ R\sin(\alpha s/R) \\ s \end{pmatrix} \tag{30}$$

R denotes the radius of the solenoid and α is related to the pitch γ by

$$\alpha = \cot\gamma \tag{31}$$

(as follows from $\dot{\mathbf{r}}(0) = (0, \alpha, 1)$).

Assume now an infinite fiber of monomers with a given pair of angles (θ, ϕ). The monomers are located at the positions $\mathbf{R}_0$, $\mathbf{R}_{\pm 1}$, $\mathbf{R}_{\pm 2}$, ... The axis of the fiber coincides with the z-axis. Assume further that we choose the values R and α so that the solenoid curve goes through all monomers. Put the monomer labeled $i = 0$ at $s = 0$ so that $\mathbf{R}_0 = (R, 0, 0)$; the subsequent monomer, $i = 1$, is at a position $\mathbf{R}_1$ given by Eq. 30 with $s = s_0$. The next monomer is located at $\mathbf{R}_2 = \mathbf{r}(2s_0)$. Finally, the position of monomer $i = -1$ is given by $\mathbf{R}_{-1} = \mathbf{r}(-s_0)$.

Now let us calculate the bond vectors between these monomers. Monomer $i = 1$ is connected to monomer $i = 0$ via

$$\mathbf{r}_0 = \mathbf{R}_1 - \mathbf{R}_0 = \begin{pmatrix} R\cos(\alpha s_0/R) - R \\ R\sin(\alpha s_0/R) \\ s_0 \end{pmatrix}$$

The separation vector between monomer $i = 2$ and $i = 1$ is given by

$$\mathbf{r}_1 = \mathbf{R}_2 - \mathbf{R}_1 = \begin{pmatrix} R(\cos(2\alpha s_0/R) - \cos(\alpha s_0/R)) \\ R(\sin(2\alpha s_0/R) - \sin(\alpha s_0/R)) \\ s_0 \end{pmatrix}$$

and that between monomer $i = 0$ and $i = -1$ by

$$\mathbf{r}_2 = \mathbf{R}_0 - \mathbf{R}_{-1} = \begin{pmatrix} R - R\cos(\alpha s_0/R) \\ R\sin(\alpha s_0/R) \\ s_0 \end{pmatrix}$$

s_0 follows from the condition of fixed linker length, i.e., $|\mathbf{r}_0| = b$. This leads to the relation

$$b^2 = 2R^2(1 - \cos(\alpha s_0/R)) + s_0^2 \tag{32}$$

We determine θ from $\cos\theta = \mathbf{r}_0 \cdot \mathbf{r}_2/|r_0^2|$, which leads to

$$\cos\theta = \frac{2R^2\cos(\alpha s_0/R)(1 - \cos(\alpha s_0/R)) + s_0^2}{2R^2(1 - \cos(\alpha s_0/R)) + s_0^2} \tag{33}$$

Finally, ϕ is the angle between normal vectors of the planes that are defined by monomers 0 and 1, i.e., $\cos\phi = \mathbf{n}_1 \cdot \mathbf{n}_2$. We obtain $\mathbf{n}_1$ and $\mathbf{n}_2$ from $\mathbf{n}_1 = \mathbf{A}/|\mathbf{A}|$ and $\mathbf{n}_2 = \mathbf{B}/|\mathbf{B}|$, where $\mathbf{A} = \mathbf{r}_0 \times \mathbf{r}_1$ and $\mathbf{B} = \mathbf{r}_2 \times \mathbf{r}_0$.

After some algebra we arrive at

$$\cos\phi = \frac{s_0^2\cos(\alpha s_0/R) + R^2\sin^2(\alpha s_0/R)}{s_0^2 + R^2\sin^2(\alpha s_0/R)} \tag{34}$$

Equations 32–34 relate α (or γ), R, and s_0 of the spiral to ϕ, θ and b.

APPENDIX B: RANDOMNESS IN THE ϕ-DISTRIBUTION

Up to now we have assumed that the values of the angles θ and ϕ are constant throughout the fiber. The resulting "ground state" configuration (unbent and untwisted linkers) is a fiber whose axis is perfectly straight. The assumption that the linker entry-exit angle θ is constant is based on the fact that it is a local property of the nucleosome core particle, and as long as the biochemical conditions are homogeneous throughout the fiber, this should be a reasonable assumption. It is known, however, that the rotational positioning is not perfect, as can be seen from the experimentally determined distribution of the linker length in chromatin (Widom, 1992). Even though a preferred rotational setting can be deduced, the width of the distribution of linker lengths will be reflected in the width of the distribution of the angle ϕ. If the rotational setting of the nucleosomes were completely random, then the chromatin configurations would correspond to particular configurations of the freely rotating chain (if we neglect excluded volume effects) (Doi and Edwards, 1986). These configurations, in turn, are those of a Gaussian chain with a persistence length $l_p = b(1 + \cos\theta)/(1 - \cos\theta)$ (the Kuhn statistical length as defined in Doi and Edwards, 1986). Note that l_p increases when θ decreases, a mechanism similar to the accordion-like unfolding of the zig-zag structure or the untwisting of the fiber with crossed linkers discussed above. In the following we will assume small variations of the rotational setting around some mean value ϕ. We consider the three cases: the solenoid, the fiber with crossed linkers, and (twisted) zig-zag structures.

Solenoids ($\phi \ll 1$, $\theta \ll 1$)

We start with the solenoidal fiber with $\phi \ll \theta \ll 1$. Then the pitch angle is small (cf. Eq. 3) and each loop of the solenoid resembles a circle. The small variations in ϕ will add up to an effective deviation $\Delta\zeta$ from the original orientation of the fiber per turn of the helix. If one has n monomers per turn it can be shown that $\langle\Delta\zeta^2\rangle = n\sigma_\phi^2$, with σ_ϕ the width of the ϕ-distribution. $\Delta\zeta$ is Gaussian with a width $\sigma_\zeta = \sqrt{n}\sigma_\phi$. With each turn the middle axis of the solenoid proceeds by a length d, where d is given by Eq. 2. We can interpret the middle axis of the solenoid as a new effective chain with bond length d, and calculate the average of the scalar product of an arbitrary pair of successive bond vectors $\mathbf{a}_i$ and $\mathbf{a}_{i+1}$ of this new effective chain:

$$\langle\mathbf{a}_i\mathbf{a}_{i+1}\rangle = \frac{d^2}{\sqrt{2\pi}\sigma_\zeta}\int d\Delta\zeta\cos(\Delta\zeta)\exp\left(-\frac{\Delta\zeta^2}{2\sigma_\zeta^2}\right)$$
$$\simeq d^2\left(1 - \frac{\sigma_\zeta^2}{2}\right), \tag{35}$$

the approximation holding for $\sigma_\zeta \ll 1$. It follows that the end-to-end distance of the chain, assuming that the solenoid has M turns (corresponding to a fiber of $N = 2\pi M/\theta$ nucleosomes), is

$$\langle L^2\rangle = \sum_{n=1}^{M}\sum_{m=1}^{M}\langle\mathbf{a}_n\mathbf{a}_m\rangle \simeq \frac{4d^2M}{\sigma_\zeta^2} \tag{36}$$

The persistence length l_p of the fiber follows from $l_p = \langle L^2\rangle/(dM)$:

$$l_p \simeq \frac{4\phi}{\theta\sigma_\phi^2}b \tag{37}$$

where we have made use of the relations $d \simeq (2\pi\phi/\theta^2)b$ (cf. Eq. 2) and $\sigma_\zeta^2 = 2\pi\sigma_\phi^2/\theta$. These results must be modified for solenoids with larger pitch angle γ ($\theta \ll \phi \ll 1$), where—as only the component $\Delta\phi\cos\gamma$ of a variation $\Delta\phi$ in the rotational angle ϕ leads to a change in the direction of the fiber (the component $\Delta\phi\sin\gamma$ leads to a twist)—one has to replace σ_ϕ by $\sigma_\phi\cos\gamma$. The resulting persistence length is given by $l_p \simeq 4b/(\sigma_\phi^2\cos^2\gamma) \simeq 4b\phi^2/(\sigma_\phi^2\theta^2)$.

Fiber with crossed linkers ($\phi \ll 1$, $\pi - \theta \ll 1$)

This case can be calculated analogously. The number of monomers per "turn" is given by $n = \pi/(\pi - \theta)$ (see above) so that $\sigma_\zeta = \sqrt{\pi/(\pi - \theta)}\sigma_\phi$. Furthermore, the bond length of the new effective chain is $d \simeq \pi\phi b/4$ (cf. Eq. 4). From Eq. 36 it follows that a fiber of $N = nM$ monomers has the mean-squared end-to-end-distance

$$\langle L^2\rangle \simeq \frac{\pi}{4}\frac{\phi^2(\pi - \theta)}{\sigma_\phi^2}b^2M \tag{38}$$

and a persistence length

$$l_p \simeq \frac{\phi(\pi - \theta)}{\sigma_\phi^2}b. \tag{39}$$

Now consider typical values for chromatin: $\phi = 36°$, $b = 20$ nm, and $\theta \approx 145°$ at 80 mM, $\theta \approx 135°$ at 15 mM, and $\theta \approx 95°$ at 5 mM (Bednar et al., 1998). Assume that the histones are located at equidistant positions but with small variations, typically ± 1 bp, i.e., $\sigma_\phi \approx 36°$; then we find $l_p \approx 20$ nm at 80 mM, $l_p \approx 25$ nm at 15 mM, and $l_p \approx 47$ nm at 5 mM.

Twisted zig-zag fiber

Finally, we consider zig-zag structures, first the case where the angle ϕ fluctuates around the mean value π (planar zig-zag). (With no fluctuations in ϕ, the zig-zag structures simply represent a perfectly flat ribbon.) Assume first that one bond is slightly rotated by $\Delta\varphi \ll 1$. As a consequence, the ribbon is deflected by an angle $\Delta\zeta_1 \simeq \sin(\theta/2)\Delta\varphi$; furthermore, the orientation of the plane defined by the ribbon rotates by an angle $\Delta\zeta_2 \simeq \cos(\theta/2)\Delta\varphi$. A long ribbon-like zig-zag structure with small fluctuations of the ϕ-angle shows individual configurations typical of a polymer with an anisotropic bending rigidity (Nyrkova et al., 1996); such a polymer has a plane of main flexibility, being highly rigid in the direction perpendicular to this plane. The anisotropy leads to two persistence lengths: an in-plane persistence length l_1, which is associated with the deflection of the ribbon within the plane of main flexibility; and an out-of-plane persistence length l_2, the typical polymer length that is needed to "forget" the orientation of the plane of main flexibility. l_1 follows from the number of monomers n_1 that is needed on average to forget the original orientation of the axis of the ribbon, $\Delta\zeta_1^2 n_1 = 4$ (the numerical value is chosen so that l_1 is compatible with the definition of the Kuhn statistical length). Thus

$$l_1 = b\cos(\theta/2)n_1 \simeq \frac{4\cos(\theta/2)}{\sin^2(\theta/2)}\frac{b}{\sigma_\phi^2} \tag{40}$$

Similarly, l_2 follows from $(2\pi)^2 = \Delta\zeta_2^2 n_2$:

$$l_2 \simeq b\cos(\theta/2)n_2 \simeq \frac{4}{\cos(\theta/2)}\frac{b}{\sigma_\phi^2} \tag{41}$$

We consider the two limiting cases. 1) $\theta = 0$: here $l_1 = \infty$ and $l_2 \simeq 4b/\sigma_\phi^2$. The configuration of the chain is that of a straight line. Variations in $\Delta\varphi$ do not affect the positions of the monomers. 2) $\theta \to \pi$: by reaching this limit the chain collapses into a configuration where it just goes back and forth between two monomer positions. Indeed, we find from the above equations that $l_1 \to 0$ and $l_2 \to \infty$.

For a twisted zig-zag structure with $\phi = \pi - \delta$ with $\delta \ll 1$ there is an inherent orientational persistence length that follows from the twist of the fiber. This leads to a length $\bar{l}_2 \simeq b\cos(\theta/2)\bar{n}_2$, where $\bar{n}_2 = 2\pi/\delta$ denotes the number of monomers per turn. Apparently the inherent twist competes with the randomly introduced one, and the out-of-plane persistence length l_2 (cf. Eq. 41) has to be replaced by $\bar{l}_2$ if $l_2 \lesssim \bar{l}_2$. The role of variations in the linker length in the case of a twisted zig-zag structure was simulated by Woodcock et al. (cf. Fig. 3 in Woodcock et al., 1993). They chose the case $\theta = 120°$ and $\delta = 360°/13 \simeq 0.48$. Using Eqs. 40 and 41 we find $l_1 \simeq 2.7b/\sigma_\phi^2$, $l_2 \simeq 8.0b/\sigma_\phi^2$, and $\bar{l}_2 = 6.5b$. It follows from our formulas that the persistence lengths l_1 and l_2 decay rapidly with σ_ϕ, a trend that can also be seen in the displayed configuration in Fig. 3 of Woodcock et al. If we choose, for instance, $\sigma_\phi = 1/2$, we find $l_p \simeq 11b$, a persistence similar to that of the fiber displayed in their Fig. 3 *b*. If we double σ_ϕ, i.e., $\sigma_\phi = 1$, we find $l_1 \simeq 3b$ so that there is no longer a well-defined fiber; a similarly disordered fiber is displayed in their Fig. 3 *d*. A closer comparison between our theoretical results and the disordered fibers shown in Woodcock et al. is not possible because in the case of the "simulated" fibers a discontinuous distribution of the values of ϕ was chosen, thereby varying the number of basepairs per linker.

APPENDIX C: PERSISTENCE LENGTHS

We calculate here the effect of linker flexibility on the persistence length of the two-angle fiber. We first calculate the zig-zag-structure where one has two different persistence lengths, the persistence length $l_p^{(in)}$ for bending within the plane of the fiber, and the length $l_p^{(out)}$ for bending out of the plane.

Zig-zag fiber: bending in plane

Assume that the ribbon is bent within its plane with a large radius R of curvature so that $R \gg b$. The linkers are bent but not twisted in this case. Up to corrections of order $(\bar{b}/R)^2$ the shape of each linker (i.e., its deviation from a straight line) is given by $u(x) = -\varepsilon x^2/\bar{b} + \varepsilon x$. This function fulfills the appropriate boundary conditions $u(0) = u(\bar{b}) = 0$ and $u'(0) = -u'(\bar{b}) = \varepsilon$. This leads to the following bending energy per linker: $E = (\kappa\bar{b}/2R^2)\cos^2(\theta/2)$. In the longitudinal direction of the fiber this corresponds to the bending of a piece of the length $\bar{b}\cos(\theta/2)$. Thus

$$A_{\text{fiber}}^{(\text{in})} = A_{\text{DNA}}\cos(\theta/2) \tag{42}$$

Zig-zag fiber: bending out of plane

This bending is accomplished by a combination of twist and bending of the linkers. Consider the two cases separately. If there is only twist allowed ($\kappa \to \infty$), then each linker has to be twisted by an angle $\bar{b}\cot(\theta/2)/R$, which leads to a twisting energy $E = C\cot^2(\theta/2)\bar{b}/2R^2$ and then in turn to the persistence length $A_{\text{twist}}^{(\text{out})} = (C/k_BT)\cos(\theta/2)/\sin^2(\theta/2)$. Now consider the case without twisting ($C \to \infty$) but with bending of the linker only. If one bends a linker out of the plane of the fiber with a radius of curvature R, it can be shown that as a result the zig-zag is deflected by an angle $\bar{b}\cos(\theta/2)/R$. If each linker is bent in such a way, the zig-zag fiber is bent out of its plane with an overall curvature of $1/R$. The bending energy per linker is $E/k_BT = A_{\text{DNA}}\bar{b}/2R^2$, leading to a persistence length $A_{\text{bend}}^{(\text{out})} = A_{\text{DNA}}/\cos(\theta/2)$. By putting the two deformation modes "in series" we find the overall persistence length for bending the zig-zag out of the plane:

$$A_{\text{fiber}}^{(\text{out})} \simeq (1/A_{\text{twist}}^{(\text{out})}1 + 1/A_{\text{bend}}^{(\text{out})})^{-1} = \frac{A_{\text{DNA}}}{\cos(\theta/2)}\frac{1}{1 + \frac{\kappa}{C}\tan^2(\theta/2)} \tag{43}$$

For small angles of θ, the bending contribution dominates and $A_{\text{fiber}}^{(\text{out})} \to A_{\text{DNA}}$ for $\theta \to 0$ (naked DNA). However, a very dense zig-zag with a value of θ close to π is bent by the twisting of the linkers, leading to a very short persistence length $A_{\text{fiber}}^{(\text{out})} \simeq (C/k_BT)\cos(\theta/2)$. Interestingly, for DNA where $\kappa \approx C$, one finds from Eq. 43 $A_{\text{fiber}}^{(\text{out})} \approx A_{\text{DNA}}\cos(\theta/2)$ over the whole range of θ-values. Thus, in this case $A_{\text{fiber}}^{(\text{in})} \approx A_{\text{fiber}}^{(\text{out})}$.

Fiber with crossed linkers

If we bend such a fiber within a given plane, then an inhomogeneous deformation pattern result where some of the linkers are oriented (nearly) parallel to the fiber while others are perpendicular. The first class of linkers will be bent, the second will be mostly twisted. The effective angle is now $\pi - \phi\cot(\theta/2)$ instead of θ (this follows from L in Table 1 with $N = 2$). As $C \approx \kappa$, the contribution to the elastic energy is approximately the same for all the linkers, leading to a persistence length

$$A_{\text{fiber}} \approx A_{\text{DNA}}\cos\left(\frac{\pi}{2} - \frac{\phi}{2}\cot(\theta/2)\right) \simeq A_{\text{DNA}}\frac{\phi}{2}\cot(\theta/2) \tag{44}$$

Using the θ-values given by Bednar et al., $\phi \approx 36°$ (and $A_{\text{DNA}} \approx 50$ nm), we find $A_{\text{fiber}} \approx 14$ nm for $\theta = 95°$ (the value at 5 mM monovalent salt), $A_{\text{fiber}} \approx 6$ nm for $\theta = 135°$ (15 mM), and $A_{\text{fiber}} \approx 5$ nm for $\theta = 145°$ (80 mM). These values are smaller than the diameter of the fiber, so it is reasonable to assume $A_{\text{fiber}} \approx 30$ nm for the persistence length of the 30-nm fiber (roughly independent of the salt concentration).

APPENDIX D: COMPARISON WITH COMPUTER SIMULATIONS

Katritch et al. performed Monte Carlo simulations of the two-angle model with flexible linkers (Katritch et al., 2000). Here we compare their results with our theoretical predictions. We first base our analysis on the results for the zig-zag case, Eq. 17, for reasons given below. Including the entropic contribution, we find the following force law:

$$f = \begin{cases} \dfrac{3k_BT}{l_p\cos(\theta/2)}\,x & \text{for } x \ll \cos(\theta/2) \\ \dfrac{12}{\sin^2(\theta/2)}\dfrac{\kappa}{b^2}[x - \cos(\theta/2)] + \dfrac{3k_BT}{l_p} & \text{for } x \gg \cos(\theta/2) \end{cases} \tag{45}$$

To allow a better comparison with the diagrams in Fig. 3 of Katritch et al. we present in Eq. 45 the force as a function of the relative extension $x = L/(\bar{b}N)$. Although most of the data of Katritch et al. were obtained assuming a (quenched) set of random values of the rotational setting of the nucleosomes, we believe that the qualitative dependence of f on θ and $\bar{b}$ should be unaffected by this assumption. Figure 3 *a* in Katritch et al. shows the dependence of the force-extension profile on the entry-exit angle $W = \pi - \theta$. It can be seen that the initial slope (entropy regime) decreases with W (increases with θ) in accordance with Eq. 45. The behavior at larger forces shows the opposite dependence, as is also predicted by Eq. 45. Finally, the crossover is shifted with increasing W to larger values; this again is in

accordance with Eq. 45. Fig. 3 *b* in Katritch et al. depicts the dependence on the linker length $\bar{b}$; here the data show no indication of a dependence of the initial slope on $\bar{b}$, and similarly for the value of the crossover, all in accordance with Eq. 45. Then, for the second regime, they find an increasing slope with decreasing linker length, also in accord the above theory.

Fig. 3 *c* of Katritch et al. shows a comparison between random rotational settings of the nucleosomes and nonrandom settings. The zig-zag case, $\phi = \pi$, has a slightly smaller initial slope than the random case and a slightly larger slope in the second linear regime, but always follows the case of random settings quite closely. This justifies the above comparison between Eq. 45—based on the zig-zag case—and the computer simulations using a random setting. Fig. 3 *c* of Katritch et al. now also allows a direct quantitative comparison. We predict from Eq. 45, for the values $\theta = 2.27$ and $\bar{b} = 40$ bp (used in Katritch et al.), that $f \simeq 0.95x$ for $x \lesssim 0.42$ and $f \simeq 14.9(x - 0.42) + 0.4$ for $x \gtrsim 0.42$ (force in piconewtons), in good agreement with their data points. (For $x \gtrsim 0.6$ the datapoints indicate an increasing slope, a result of nonlinear effects not taken into account in our theory.)

Finally, Katritch et al. also provide data points for the case $\phi = 0.35$ and $\theta = 2.27$. We find from Eq. 27 that one has $f \simeq 4.9x$ for $x \lesssim 0.1$ and $f \approx 8.6(x - 0.1) + 0.5$ for $x \gtrsim 0.1$. (Here $x \equiv L/\bar{b}N$, and $x_0 \equiv L_0/\bar{b}N = (\phi/2)\cot(\theta/2) \approx 0.1$.) This result overestimates the entropic contribution, as can be seen by comparison with the $Tw = 20°$ curve in Fig. 3 *c* of Katritch et al. (data points are missing for $x < 0.2$ but the force at $x = 0.2$ is smaller than 1 pN). The reason is probably the underestimation of the persistence length of the fiber l_P, assumed here to be of the order of the fiber thickness. The real value could be larger, as this set of angles corresponds to an extremely dense fiber where excluded volume effects become rather important. The simulation data for this set of angles is not found to be in good agreement with the experimental force-extension characteristics. This might be attributed to the small value of the entry-exit angle (130° instead of 85° as suggested by the electron cryomicrographs, Bednar et al., 1998); if we use $\theta = 95°$ and $\phi = 36°$ (as above) we find $f \simeq 1.4x$ for $x \lesssim 0.3$ and $f \approx 4.7(x - 0.3) + 0.2$ for $x \gtrsim 0.3$, which is closer to the experimental curve.

We thank J. Widom for many valuable discussions and for a critical reading of the manuscript. We acknowledge useful conversations with J.-L. Sikorav and F. Livolant.

This work was supported by the National Science Foundation under Grant DMR-9708646.

REFERENCES

Bednar, J., R. A. Horowitz, J. Dubochet, and C. L. Woodcock. 1995. Chromatin conformation and salt-induced compaction: 3-dimensional structural information from cryoelectron microscopy. *J. Cell. Biol.* 131: 1365–1376.

Bednar, J., R. A. Horowitz, S. A. Grigoryev, L. M. Carruthers, J. C. Hansen, A. J. Koster, and C. L. Woodcock. 1998. Nucleosomes, linker DNA, and linker histone form a unique structural motif that directs the higher-order folding and compaction of chromatin. *Proc. Natl. Acad. Sci. USA.* 95:14173–14178.

Butler, P. J. G., and J. O. Thomas. 1998. Dinucleosomes show compaction by ionic strength, consistent with bending of linker DNA. *J. Mol. Biol.* 281:401–407.

Cluzel, P., A. Lebrun, C. Heller, R. Lavery, J. L. Viovy, D. Chatenay, and F. Caron. 1996. DNA: an extensible molecule. *Science.* 271:792–794.

Crothers, D. M., J. Drak, J. D. Kahn, and S. D. Levene. 1992. DNA bending, flexibility, and helical repeat by cyclization kinetics. *Methods Enzymol.* 212:3–29.

Cui, Y., and C. Bustamante. 2000. Pulling a single chromatin fiber reveals the forces that maintain its higher-order structure. *Proc. Natl. Acad. Sci. USA.* 97:127–132.

de Gennes, P.-G. 1979. Scaling Concepts in Polymer Physics. Cornell University Press, Ithaca, NY.

Doi, M., and S. F. Edwards. 1986. The Theory of Polymer Dynamics. Clarendon Press, Oxford.

Finch, J. T., and A. Klug. 1976. Solenoidal model for superstructure of chromatin. *Proc. Natl. Acad. Sci. USA.* 73:1897–1901.

Fraden, S., and R. D. Kamien. 2000. Self-assembly in vivo. *Biophys. J.* 78:2189–2190.

Hagerman, P. J. 1988. Flexibility of DNA. *Annu. Rev. Biophys. Biophys. Chem.* 17:265–286.

Horowitz, R. A., D. A. Agard, J. W. Sedat, and C. L. Woodcock. 1994. The three-dimensional architecture of chromatin in situ: electron tomography reveals fibers composed of a continuously variable zig-zag nucleosomal ribbon. *J. Cell. Biol.* 125:1–10.

Katritch, V., C. Bustamante, and W. K. Olson. 2000. Pulling chromatin fibers: computer simulations of the direct physical micromanipulation. *J. Mol. Biol.* 295:29–40.

Khrapunov, S. N., A. I. Dragan, A. V. Sivolob, and A. M. Zagariya. 1997. Mechanisms of stabilizing nucleosome structure. Study of dissociation of histone octamer from DNA. *Biochim. Biophys. Acta.* 1351:213–222.

Klenin, K. V., A. V. Vologodskii, V. V. Anshelevich, V. Y. Klishko, A. M. Dykhne, and M. D. Frank-Kamenetskii. 1989. Variance of writhe for wormlike DNA rings with excluded volume. *J. Biomol. Struct. Dyn.* 6:707–714.

Leuba, S. H., G. Yang, C. Robert, B. Samori, K. van Holde, J. Zlatanovam, and C. Bustamante. 1994. Three-dimensional structure of extended chromatin fibers as revealed by tapping-mode scanning force microscopy. *Proc. Natl. Acad. Sci. USA.* 91:11621–11625.

Livolant, F., and A. Leforestier. 2000. Chiral discotic columnar germs of nucleosome core particles. *Biophys. J.* 78:2716–2729.

Luger, K., A. W. Mäder, R. K. Richmond, D. F. Sargent, and T. J. Richmond. 1997. Crystal structure of the nucleosome core particle at 2.8A resolution. *Nature.* 389:251–260.

Marko, J. F. 1998. DNA under high tension: overstretching, undertwisting, and relaxation dynamics. *Phys. Rev. E.* 57:2134–2149.

Marko, J. F., and E. D. Siggia. 1997. Driving proteins off DNA using applied tension. *Biophys. J.* 73:2173–2178.

Nyrkova, I. A., A. N. Semenov, J.-F. Joanny, and A. R. Khokhlov. 1996. Highly anisotropic rigidity of "ribbon-like" polymers. I. Chain configuration in dilute solutions. *J. Phys. II France.* 6:1411–1428.

Plewa, J. S., and T. A. Witten. 2000. Conserved linking in single- and double-stranded polymers. *J. Chem. Phys.* 112:10042–10048.

Raspaud, E., I. Chaperon, A. Leforestier, and F. Livolant. 1999. Spermine-induced aggregation of DNA, nucleosome, and chromatin. *Biophys. J.* 77:1547–1555.

Schiessel, H., J. Widom, R. F. Bruinsma, and W. M. Gelbart. 2001. Polymer reptation and nucleosome repositioning. *Phys. Rev. Lett.* (in press).

Schlick, T. 1995. Modeling superhelical DNA: recent analytical and dynamic approaches. *Curr. Opin. Struct. Biol.* 5:245–262.

Smith, S. B., Y. Cui, and C. Bustamante. 1996. Overstretching B-DNA: the elastic response of individual double-stranded and single-stranded DNA molecules. *Science.* 271:795–799.

Stryer, L. 1995. Biochemistry, 4th Ed. Freeman, New York. 420–421.

Thoma, F., Th. Koller, and A. Klug. 1979. Involvement of the histone H1 in the organization of the nucleosome and of the salt-dependent superstructures of chromatin. *J. Cell. Biol.* 83:403–427.

van Holde, K. E. 1989. Chromatin. Springer Verlag, New York.

van Holde, K., and J. Zlatanova. 1995. Chromatin higher order structure: chasing a mirage? *J. Biol. Chem.* 93:8373–8376.

van Holde, K., and J. Zlatanova. 1996. What determines the folding of the chromatin fiber? *Proc. Natl. Acad. Sci. USA.* 93:10548–10555.

Widom, J. 1986. Physicochemical studies of the folding of the 100A nucleosome filament into the 300A filament. *J. Mol. Biol.* 190:411–424.

Widom, J. 1989. Toward a unified model of chromatin folding. *Annu. Rev. Biophys. Biophys. Chem.* 18:365–395.

Widom, J. 1992. A relationship between the helical twist of DNA and the ordered positioning of nucleosomes in all eukaryotic cells. *Proc. Natl. Acad. Sci. USA.* 89:1095–1099.

Widom, J. 1998. Structure, dynamics, and function of chromatin in vitro. *Annu. Rev. Biophys. Biomol. Struct.* 27:285–327.

Widom, J., and A. Klug. 1985. Structure of the 300A chromatin filament: x-ray diffraction from oriented samples. *Cell.* 43:207–213.

Woodcock, C. L., S. A. Grigoryev, R. A. Horowitz, and N. Whitaker. 1993. A chromatin folding model that incorporates linker variability generates fibers resembling native structures. *Proc. Natl. Acad. Sci. USA.* 90: 9021–9025.

Yao, J., P. T. Lowary, and J. Widom. 1990. Direct detection of linker DNA bending in defined-length oligomers of chromatin. *Proc. Natl. Acad. Sci. USA.* 87:7603–7607.